Effect of Dielectric Confinement on Energetics of Quantum Metal Films: Analysis of Calculation Results

V. V. Pogosov

Zaporizhzhia Polytechnic National University,
64 Zhukovsky Str.,
UA-69063 Zaporizhzhya, Ukraine

We examine thin film on a dielectric substrate (vacuum/Al/SiO$_2$) in the stabilized jelly model. We investigate the surface and size effects on the effective potential and the electron work function for the weak quantization regime. We find that a dielectric environment generally leads to the decrease of the work function. We introduce the position of a conduction band for the dielectric as the input parameter in the self-consistency procedure. The effect of dielectric confinement for the energy characteristics of the asymmetric metal–dielectric sandwiches is reduced to only by the surface-area weighted average value of the dielectric constants. This conclusion follows from the application of the Gauss theorem for a conducting sphere with an inhomogeneous dielectric coating. The flow of electrons from the dielectric face to the vacuum one due to the contact-potential difference manifests itself in the appearance of a potential barrier above the vacuum level or positive values of the effective potential. The barrier height depends on the used local or nonlocal approximation of the exchange–correlation energy. The nontrivial origin and behaviour of the calculated effective potential on the vacuum side of the film, as well as the reasons for it, are discussed. In the focus of our representations, we analyse the recent results of measurements of the contact-potential difference depending on the number of Si atoms deposited on the free face of ytterbium nanofilms on the Si(111) substrates. Comparison and discrepancies between our self-consistent calculations for simple metals and these experiments are discussed.

Key words: surface electronic phenomena, work function, surface potential, contact potential difference, metal–insulator interfaces, sandwiches, films,

Corresponding author: Valentyn Val'terovych Pogosov
E-mail: vpogosov@zntu.edu.ua

jelly models.

В моделю стабільного желе для режиму слабкого квантування досліджено вплив поверхневого та розмірного ефектів на ефективний потенціял і роботу виходу електрона металевої наноплівки на діелектричній підкладинці (вакуум/Al/SiO₂). Виявлено, що контакт з діелектриком, як правило, приводить до зменшення роботи виходу електрона. У процедурі самоузгодження в якості вхідного параметра введено положення зони провідности для діелектрика. Вплив контакту з діелектриками на енергетичні характеристики асиметричних метал-діелектричних сандвічей зводиться лише до середнього зваженого за площею контакту значення діелектричних проникностей обкладинок. Цей результат є наслідком застосування Ґаусової теореми для провідної сфери з неоднорідним діелектричним покриттям. Зсув електронів у плівці від діелектричної підкладинки до вакуумного інтерфейсу за рахунок контактної ріжниці потенціялів проявляється у появі потенціяльного бар'єру над вакуумним рівнем або позитивних значень ефективного потенціялу. Висота бар'єру залежить від використовуваного локального або нелокального наближення для обмінно-кореляційної енергії. Обговорюються нетривіяльна поведінка розрахованого ефективного потенціялу на вакуумній стороні плівки, а також причини цього. На основі одержаних результатів проаналізовано нещодавні результати мірянь контактної ріжниці потенціялів в залежності від кількости атомів Si, нанесених на вільну грань наноплівок ітербію на підкладинці Si(111). Обговорюються порівняння та розбіжності між нашими самоузгодженими розрахунками для простих металів і цими експериментами.

Ключові слова: поверхневі явища, робота виходу електрона, поверхневий потенціял, контактна ріжниця потенціялів, метал-діелектричні інтерфейси, сандвічі, плівки, модель стабільного желе.

(Received August 12, 2023; in final version, August 13, 2023)

1. INTRODUCTION

Thin films of metals, dielectrics and semiconductors are widely used in many fields of technology, primarily in micro- and nanoelectronics. Physical processes in thin films proceed differently than in bulk materials. As a result, film elements have characteristics that differ from those of bulk samples and allow one to observe effects that are not characteristic of bulk samples.

Films in the nanometer range exhibit the size and quantum effects. The Friedel oscillations of the electron density are always present in a metallic film. Their amplitude depends on the contact with the substrate. For thick films, these oscillations are localized near the surface and decay deep into the bulk of the film. With a decrease in the film thickness, the quantum-size density oscillations (standing waves) begin to appear, superimposed on the Friedel oscillations. In addition,

the substrate material can have a significant effect on the energy characteristics of thin films [1, 2]. One of the fundamental characteristics of metal nanostructures is the electron work function.

The possibility of light localization makes it possible to demonstrate, based on the surface plasmon resonance spectroscopy, their efficiency and performance as the hybrid plasmonic waveguides, the biological and chemical sensors, nanoantennas, metamaterials, and the highly reflective coatings (see Refs. [3–5] and references therein).

The complexity of obtaining objects and measurement methods is evidenced by a relatively small number of experiments devoted, as a rule, to quantum size effects [5–12].

Various approaches and models make it possible to calculate the electron structure of the slabs suspended in vacuum and consisting of several monolayers (ML), finite in one direction and quasi-continuous in two other directions [13–17]. Within the framework of the density functional theory and the stabilized jelly, we calculated the electron characteristics of metal–dielectric nanosandwiches for the strong quantization regime [18–21].

The aim of the present work is the calculation and analysis of the energy diagram, the electron work function, and near-surface space distribution of a one-electron effective potential for an aluminium film on a promising substrate SiO_2 [22].

To control calculations by the Kohn–Sham method of the energy diagram of a metal film with an inhomogeneous dielectric coating, the simplest electrostatic analogue of the problem, for example, about a point charge [23] at the interface with several dielectrics, is required. Subsequently, we will present its solution in the form necessary for our purposes, as it was proposed in [21].

2. ELECTROSTATIC ANALOGUE

Let us consider a conducting sphere in an inhomogeneous dielectric environment: from a straight line passing through the centre of the sphere of radius R and charge Q, the i half-planes diverge fan-shaped, forming dihedral angles $\beta_1, \beta_2, ..., \beta_i$ such that (Fig. 1, a)

$$\sum_i \beta_i = 2\pi \,.$$

In the region $r > R$, the space inside each of the corners is filled with homogeneous dielectrics with constants $\varepsilon_1, \varepsilon_2, ..., \varepsilon_i$, respectively. Determining the potential on the surface of a sphere, we first assume that the general form of the solution for the potential in the region $r \geq R$ has the form

$$\phi_i = C_i \, Q/r \,.$$
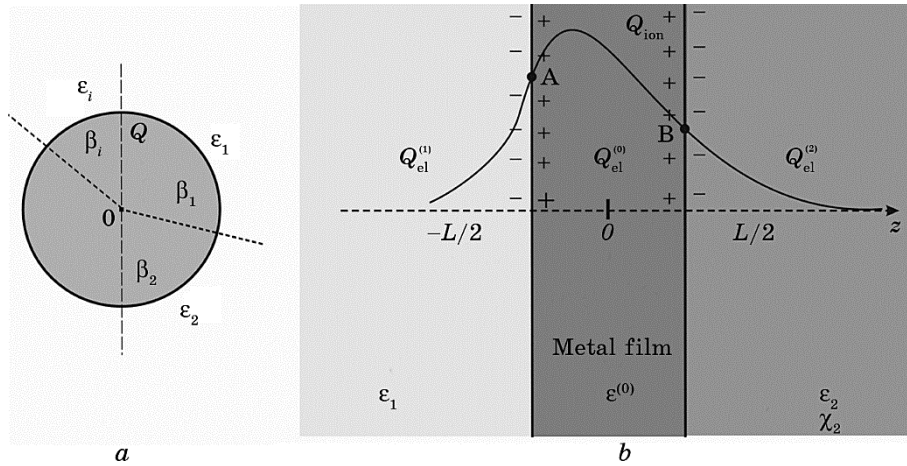
Fig. 1. The illustrations of a conducting sphere in contact with dielectrics (*a*) (the planes separating the dielectrics are perpendicular to the plane of the figure), metal film in the contacts (*b*).

From the boundary conditions for the equality of the potential at the corresponding boundaries with dielectrics, we obtain

$$\phi_1^R = \phi_2^R = \ldots = \phi_i^R \Rightarrow C_i = C \,.$$

The unknown coefficient C is determined by the Gauss theorem

$$\oint_S \mathbf{D}d\mathbf{S} = 4\pi Q \,. \tag{1}$$

To find the area of a segment $S_i = \alpha_i S$ on a radius R (α_i is the fraction of the surface covered by a dielectric with a constant ε_i), we introduce a *z*-axis along the line of separation of the dielectrics. Then, according to the Cavalieri's principle, each *i*-th area will be determined by the angle β_i (Fig. 1, *a*) or

$$\alpha_i = \frac{\beta_i}{2\pi} \,,$$

and the integral in Eq. (1) is divided into *i* parts

$$S \sum_i D_i^n \alpha_i = 4\pi Q \,. \tag{2}$$

Substituting the area of the sphere and $D_i^n = \varepsilon_i C Q / R^2$, we get $C = 1/\tilde{\varepsilon}$, where

$$\tilde{\varepsilon} \equiv \sum_i \varepsilon_i \alpha_i \,. \tag{3}$$

Thus, the area-weighted average dielectric constant $\tilde{\varepsilon}$ is introduced into the theory, and the potential of the sphere surface $\phi^R = Q/(\tilde{\varepsilon}R)$ is common for all contacts with dielectrics, as well as the asymptotics of the potential in the limit $r/R \gg 1$:

$$\phi(r) = \frac{Q}{\tilde{\varepsilon}r}. \tag{4}$$

For a metal sphere in contact with two dielectrics (inhomogeneous coating), we have

$$\tilde{\varepsilon} = \varepsilon_1\alpha_1 + \varepsilon_2\alpha_2. \tag{5}$$

Mentally 'flattening' the metal ball [21], let us consider a metal film. In the Cartesian co-ordinate system, it is more convenient to use a macroscopic metal cube [24] with a volume $\Omega = L_x \times L_y \times L_z$, symmetrically located between the dielectrics in the plane xy. Then, flattening the cube along the z-axis, we consider a slab with a thickness L (Fig. 1, b). Neglecting the ends, the total film area S, parameters α and $\tilde{\varepsilon}$ have the trivial form:

$$S = 2L_xL_y + O\left(\frac{L}{L_x}\right), \; \alpha_1 = \alpha_2 = \frac{1}{2}, \; \tilde{\varepsilon} = \frac{1}{2}(1 + \varepsilon_2). \tag{6}$$

Next, we use the Kohn–Sham method to analyse the energy diagram for the passive contact of film with an insulator. Previously, we considered such a problem for a quantum metal film in dielectric environment [18–20].

3. MODEL OF FILM

For an electrically neutral metal film (slab), the total charge of the subsystem of conduction electrons and ions is zero. Therefore, there is no electric field at infinity.

In the stabilized jelly model, the field is nonzero only near the surface, where the electron density profile $n(z)$ changes from the bulk value in metal bulk $\bar{n} = \bar{\rho}$ to zero beyond the boundary of the positive ion charge distribution given in a stepwise form

$$\rho(z) = \begin{cases} 0, \; z < -L/2, \\ \bar{n}, \; |z| \le L/2, \; \bar{n} = \dfrac{1}{(4/3)\pi r_{\mathrm{s}}^3}, \\ 0, \; z > L/2. \end{cases} \tag{7}$$

Let us conventionally divide the space distribution of conduction

electrons into regions (Fig. 1, *b*):

$$n(z) = n_1(z) + n_0(z) + n_2(z),$$

in which the charges are accumulated

$$Q_{el}^{(1)} = -e\frac{1}{2}S\int_{-\infty}^{-L/2} n_1(z)\,dz,\; Q_{ion} = +e\frac{1}{2}S\int_{-L/2}^{L/2}\rho(z)\,dz,$$

$$\tag{8}$$

$$Q_{el}^{(0)} = -e\frac{1}{2}S\int_{-L/2}^{L/2} n_0(z)\,dz,\; Q_{el}^{(2)} = -e\frac{1}{2}S\int_{L/2}^{\infty} n_2(z)\,dz,$$

where *e* is the unit positive charge. The sum of charges satisfies the electrical-neutrality condition

$$Q_{ion} + Q_{el}^{(1)} + Q_{el}^{(0)} + Q_{el}^{(2)} = 0. \tag{9}$$

The spatial electron distribution is determined by the Poisson equation

$$\nabla^2\phi = -4\pi e\frac{\nu(z)}{\varepsilon(z)}, \tag{10}$$

$$\nu(z) = n(z) - \rho(z).$$

The step function

$$\varepsilon(z) = \begin{cases} \varepsilon_1, z < -L/2, \\ \varepsilon^{(0)}, |z| \le L/2, \\ \varepsilon_2, z > L/2 \end{cases} \tag{11}$$

fixes the area of contacts with vacuum and dielectric; $\varepsilon^{(0)} = 1$ (ions and electrons in a metal are always in a vacuum).

The count of the potential is selected from its value $\phi = 0$ at a sphere of infinite radius (this is true for a finite sample of arbitrary shape).

From the joint solution of the Kohn–Sham equations and the Poisson equation (10), the equilibrium profiles $n(z)$, $\phi(z)$, $v_{eff}(z)$ and the electron work function W under the condition of the co-ordinate-independent chemical potential of electrons are found:

$$\mu(\varepsilon_1, \varepsilon_2, x, y, z) = \text{const} = -W. \tag{12}$$

Thus, condition (12) also fixes the mutual influence of dielectrics on the asymptotic potential $v_{eff}(z)$ behaviour [25].

The one-electron effective potential is defined as the sum

$$v_{\text{eff}}(z) = e\phi(z) + v_{\text{xc}}(z) + \left\langle \delta v \right\rangle_{\text{WS}} \theta(L/2 + z)\theta(L/2 - z), \qquad (13)$$

where v_{xc} is the exchange–correlation potential in the local density approximation (LDA), $<\delta v>_{\text{WS}}$ is the stabilization potential (zero point energy), and $\theta(z)$ is the Heaviside unit function.

It is assumed that the electron escaping from the metal film is accompanied by a spherically symmetric hole, which is trapped in the image plane and spreads out within this plane as the electron moves apart from the surface [26].

In the version of [20], the Ritz method was used to obtain an analytical expression for the nonlocal Coulomb potential of a hole, which was then matched on the image plane with the local exchange–correlation potential calculated by the Kohn–Sham method under condition (12). Thus, the effective potential is self-consistently and asymmetrically matched outside the film with the image potentials ('short-range asymptotics' for the faces)

$$+\frac{e^2}{4\varepsilon_1(z + L/2)} \text{ and } -\frac{e^2}{4\varepsilon_2(z - L/2)}. \qquad (14)$$

For thin films, in which the bottom of the effective potential is not flat due to the Friedel and size oscillations of the electron density, the work function, as for clusters of atoms, is defined as

$$W = -\varepsilon_F. \qquad (15)$$

Here, the Fermi energy $\varepsilon_F < 0$ is counted down the energy scale from a value $\phi = 0$ on infinity.

The convergence problems of the iterative procedure significantly complicate the calculations for large film thicknesses, when the quantum-size oscillations of the work function are negligibly small.

For thick films, in which the bottom of the one-electron effective potential in film is flat in the vicinity of $z = 0$, the work function can be found, as in a semi-infinite metal, in the form:

$$W = -\bar{v}_{\text{eff}} - \bar{\varepsilon}_F, \ \bar{v}_{\text{eff}} = e\bar{\phi} + \bar{v}_{\text{xc}} + \left\langle \delta v \right\rangle_{\text{WS}}, \ \bar{\varepsilon}_F = (\hbar^2/(2m))(3\pi^2\bar{n})^{2/3}, \quad (16)$$

where $\bar{v}_{\text{eff}}$ is the bottom of the conduction band in a massive metal, $\bar{\varepsilon}_F > 0$ is the Fermi energy of a homogeneous degenerate electron gas in the Sommerfeld model (here, it is already generally accepted to choose $\bar{\varepsilon}_F$ a reading up the energy scale from $\bar{v}_{\text{eff}} < 0$).

If the terms $\bar{\phi}$ and $\bar{v}_{\text{xc}}$ are of Coulomb origin, then, in addition to the exchange–correlation contribution, $<\delta v>_{\text{WS}}$ also contains the non-Coulomb contribution of $\bar{\varepsilon}_F$.

In Figure 1, *b* pluses and minuses show the distribution of charges

providing the ordinary dipole barrier $(-e\bar{\phi})$ near faces.

4. CALCULATION RESULTS AND DISCUSSION

Calculations are made for the asymmetric and symmetric 'sandwiches'

$$
\begin{aligned}
&1 : \{\varepsilon_1 \mid \text{Al} \mid \varepsilon_2\}, \\
&2 : \{\tilde{\varepsilon} \mid \text{Al} \mid \tilde{\varepsilon}\}, \ \tilde{\varepsilon} = \tfrac{1}{2}(\varepsilon_1 + \varepsilon_2), \\
&3 : \{\varepsilon_1 \mid \text{Al} \mid \varepsilon_2, \chi_2\}
\end{aligned} \tag{17}
$$

in two approximations ($\chi_2 = 0$ and $\chi_2 \neq 0$): vacuum on the left; polycrystalline Al film ($r_s = 2.07a_0$, a_0 is the Bohr radius) of thickness $L = 32a_0 = 7$ ML in the centre; SiO_2 on the right ($\varepsilon_2 = 4$, $\chi_2 = 1.1$ eV) within the framework of our approaches [18−20]. For sandwich 3, a non-local exchange−correlation potential was used [19].

Figures 2 and 3 demonstrate the most interesting fragments of the equilibrium profiles of the electron density and electrostatic potential. The tails of electronic profiles 1 and 3 almost coincide, but at the same time, they shift asymmetrically relative to the symmetrical sandwich 2 towards the dielectric. For all cases, the electronic charge $Q_{\text{el}}^{(0)}$ in the $|z| \leq L/2$ area remains almost the same. This is manifested in the equality of the potential for points A and B in Fig. 3, which exactly corresponds to theorem (1) and result (4).

The tails in Figure 2, which make up the charges $Q_{\text{el}}^{(1)}$ and $Q_{\text{el}}^{(2)}$, visually differ slightly. However, these tails are present in the Poisson equation with different weights: $n_1(z)/\varepsilon_1$ and $n_2(z)/\varepsilon_2$. Due to the sig-
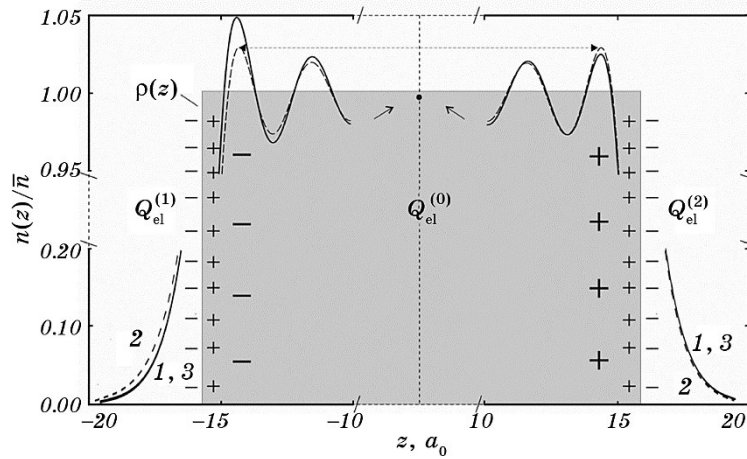

Fig. 2. Calculated electron density profiles in accordance with the notation (17).
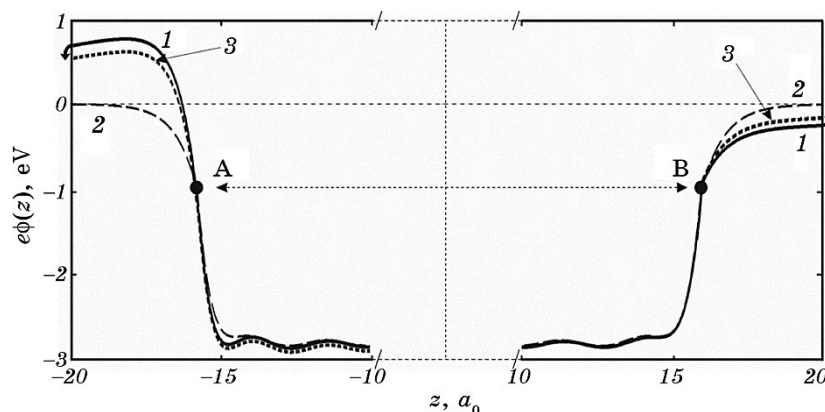
Fig. 3. Calculated electrostatic potential profiles.

nificant difference in ε_1 and ε_2, a small difference in n_1 and n_2 cannot fundamentally affect the wings of the potential $\phi(z)$ (Fig. 3) and the Maxwellian stress tensor in the system.

The boundary conditions for $\phi(z)$ provide reliable equipotential surfaces passing through points A, B, and $|z| = \infty$. For sandwich *2*, the wings of the potential are expectedly symmetrical. For a sandwich in approximations *1* and *3*, as well as for small film thicknesses, the potential wings behave quite differently.

In Figure 3, the potential wings in the dielectric for *1* and *3* lie lower than for the symmetrical sandwich *2* and tend to $\phi = 0$, much more slowly. It is important not only that in this region the action of the charge $(Q_{\text{ion}} + Q_{\text{el}}^{(0)}) > 0$ predominates, but also its spatial distribution inside the film. Indeed, the electronic charge inside the film is distributed asymmetrically (the extreme peak on the left is higher than the extreme peak on the right), which creates an additional dipole between the left and right faces (it is indicated in Fig. 2 by large pluses and minuses). This leads to the fact that in vacuum the potential $\phi(z)$ increases sharply (the effect of two infinitely charged 'planes'), exceeding the potential for a symmetrical sandwich, crosses $\phi = 0$, reaches a maximum, crosses again $\phi = 0$ and tends to $\phi = 0$ at infinity from the lower half-plane. Thus, Figure 2 shows the flow of electrons inside the film from the dielectric side to the vacuum side due to the contact potential difference. In turn, this is clearly manifested in the appearance of a potential barrier above the vacuum level or, in other words, positive values on the left wing of the potential in Fig. 3. The contact potential difference is determined by the dependence of the work function [27] of half-infinite Al in passive contact with a dielectric (Fig. 4) or, equivalently, of an 'infinitely' thickness film in identical faces with constant ε.
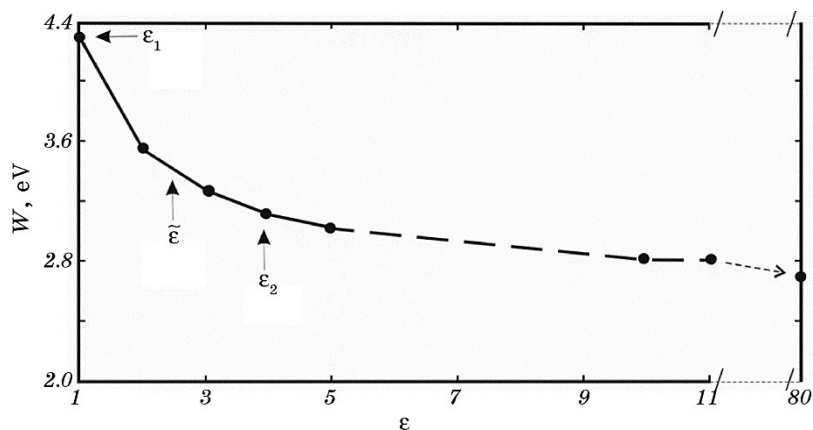
Fig. 4. The work function vs dielectric coating in the absence of size oscillations.
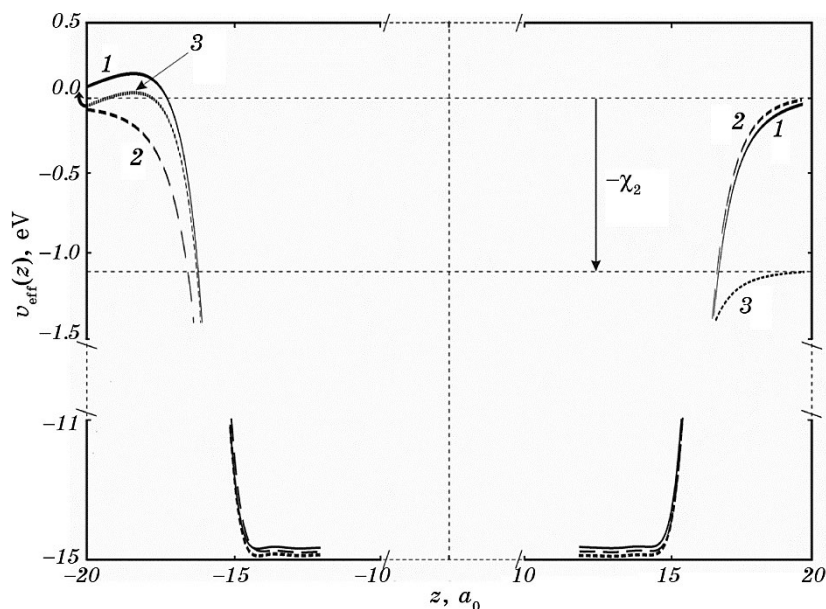

Fig. 5. Calculated effective potential profiles.

The difference in versions *1* and *3* did not affect the value of $\varepsilon_F = -3.17$ eV in **(15)**. For comparison, the work function **(16)** exceeds this value by only 5% (weak quantization regime). On the other hand, the difference in the versions noticeably changed the wings of the potential $v_{eff}(z)$ (**Fig. 5**). The use of the nonlocal exchange–correlation potential in the iterative procedure led to a significant suppression in

vacuum of the potential barrier of the effective potential (now its height is only $0.16\,\text{eV}$). For the electrostatic potential, this change is much smaller (dependences *1* and *3* are compared in Fig. 3). In the $z < -L/2$ area, effective electric field

$$E_{\text{eff}}(z) = -\nabla v_{\text{eff}}(z) \, / \, e$$

changes sign twice. In theorem (1), apparently, one should make the change $\mathbf{D} \to \mathbf{D}_{\text{eff}}$.

In a metal, it is not enough to confine oneself to taking into account only the electrostatic potential calculated in accordance with the principle of superposition; the prevailing contribution to energy is made by the exchange–correlation potential due to the small distance between electrons r_{s} [26]. Therefore, at distances smaller than the lateral dimensions of the film ($z \ll L_x$), both asymptotics (14) work. At a much greater distance from the faces, when the exchange–correlation effects become negligible with increasing distance r_{s}, the superposition principle is dominant. In this case, one 'long-range' asymptotics of the form (4) with a weighted average dielectric constant $\tilde{\varepsilon}$ should work. Numerical investigation of the asymptotic behaviour of the potential does not allow the calculation algorithm instability near the vacuum level.

To analyse the complex behaviour of the potential, it is necessary to go beyond the model with stepwise distributions of a homogeneous positively charged background (7) and the dielectric constant in (11). It is also necessary to take into account not only the response of the electronic, but also the ionic subsystem to the presence of a dielectric. If atomic planes are introduced into the film model, then the interplanar distances will be determined by the balance of forces on the left and right on each of them. The effective force acting from the outside on the film is due to the inhomogeneous distribution of electrons and should lead to its compression in z direction. As the thickness decreases, the role of alternating deformation increases. Most likely, this will lead to some refinement of the electron work function, but not a significant change in the potential wings.

Modernization of the stepwise manner into function $\varepsilon(z)$ (11) can be carried out using, for example, a more realistic inclusion function in the region of dielectrics:

$$\varepsilon(z) = \varepsilon^{(0)} + \begin{cases} (\varepsilon_1 - \varepsilon^{(0)})(1 - \exp[(z + L/2) \, / \, a_1]), & z < -L/2, \\ (\varepsilon_2 - \varepsilon^{(0)})(1 - \exp[-(z - L/2) \, / \, a_2]), & z > L/2. \end{cases} \tag{18}$$

In general, the parameters $a_{1,2}$ should be comparable with the diameters of dielectric atoms on both sides of the film. Numerically, this somewhat softens the asymmetry of the dielectric near the surface and lowers the potential barrier in Figs. 3 and 4. The final answer about the

presence of anomalies in the behaviour of the potential near the surface can be given by a detailed analysis of the experimental dependences of the STM tunnelling current on the probe-surface distance. It is possible that the variation of the potential affects the rate of adsorption on the free plate of the film, which is a sensitive point in the design of sensors.

In a recent work [12], it was reported on the study by the Kelvin method (contact potential difference) of ytterbium nanofilms at Si (111) substrates. The probe fixed changes in the average surface potential $e\Delta\varphi$ (or local work function of electrons) depending on the number of Si atoms deposited on the free Yb face. Silicon was deposited in portions up to approximately 1 ML.

In our calculation scheme, the value $e\Delta\varphi$ corresponds to the change in the effective potential on the image plane $v_{\text{eff}}(z = z_0)$, $z_0 < -L/2$ (see Table II in [28]). The value ε_1 in the experiment [12] can be estimated using the Clausius−Mossotti relation, using the polarizability of the Si atom $(10.17a_0^3)$ and detailed information about the islands. Then, formula (5) will look like

$$\tilde{\varepsilon} = \sum_j \varepsilon_j \alpha_j + \varepsilon_2/2 \,, \tag{19}$$

where j is the number of Si islands on the left face. The transition to vacuum means $\varepsilon_j = 1$, $\sum_j \alpha_j = 1/2$ that will lead to expression (6).

On the one hand, the use of such a concept as the dielectric constant for dielectric nanoislands is doubtful, but, on the other hand, the use of formula (19) leads to its value being greater than that according to formula (18) for $\varepsilon_1 = 1$. If we also use Fig. 4 (metal in this case is not important, but it is important that the contact is passive), it turns out that the work function: the total energy (15) and (16) should decrease with the appearance of adsorbent islands.

In Ref. [12], the value $e\Delta\varphi$ for Yb films with a thickness of 7.8 and 16 ML, on the contrary, increases by approximately 0.02 eV with an increase in the Si coverage.

The reasons for the opposite change in $e\Delta\varphi$ and W have already been discussed by us earlier [27, 28] (see, for example, formula (23) in [27]). There are additional reasons for the discrepancy between theory and experiment: (i) the film is not continuous and homogeneous, this is especially evident for a film with a thickness of 7.8 ML, (ii) the oscillations of the Fermi energy are consistent with the oscillations of the electron pressure on the walls, which leads to size oscillations of the film thickness itself and of the potential wings, one of which is used for measurements, (iii) when using a probe, edge effects have an influence. Here, one should also point to the work [29] and the book [30], where it was reported on the measurement by means of photoelectron

spectroscopy of nonmonotonic curves of the change in the work function with a decrease in the size of Ag, Al, Fe, Mg particles deposited on a quartz substrate.

5. CONCLUSIONS

This paper presents the results of the numerical solution of the many-electron problem: self-consistent profiles of the electron density, potentials, and electron work function for 7 ML thickness polycrystalline Al film deposited on a passive insulator SiO_2 (asymmetric metal−dielectric sandwich). An analysis based on the Gauss theorem points to the universality of using the constant $\tilde{\varepsilon}$, weighted average over the surface area of the contacts with dielectrics. Comparison with the value of the electrostatic potential calculated by the Kohn−Sham method for the film covered homogeneous dielectric $\tilde{\varepsilon}$ confirms the conclusions of classical electrodynamics.

The effective force acting on the film from the outside is due to the inhomogeneous distribution of electrons and should lead to its size deformation.

The flow of electrons from the side of the dielectric to the vacuum side due to the contact potential difference manifests itself in the appearance of a barrier above the vacuum level or positive values of the effective potential. The barrier height depends on the used local or non-local approximation of the exchange−correlation energy. Therefore, the answer about the presence of anomalies in the behaviour of the potential should be sought in the behaviour of the STM tunnelling current near the vacuum face of the film. The variation of the potential here affects the rate of adsorption on the free plate of the film, which is a sensitive point in the design of sensors.

The work function and lifetime of a positron in the surface states of a metal film is sensitive to the presence of a potential barrier and, if its presence is experimentally confirmed, this will require a critical revision of the measured values.

REFERENCES

1. H. Kawano, *Prog. Surf. Sci.*, **97**, No. 1: 100583 (2022).
2. R. Otero, A. L. Vázquez de Parga, and J. M. Gallego, *Surf. Sci. Rep.*, **72**, No. 3: 105 (2017).
3. D. Yu. Fedyanin, D. I. Yakubovsky, R. V. Kirtaev, and V. S. Volkov, *Nano Lett.*, **16**, No. 1: 362 (2016).
4. A. K. Sarychev, A. Ivanov, A. N. Lagarkov, I. Ryzhikov, K. Afanasev, I. Bykov, G. Barbillon, N. Bakholdin, M. Mikhailov, A. Smyk, A. Shurygin, and

A. Shalygin, *Phys. Rev. Appl.*, **17,** No. 4: 044029 (2022).

5.   A. V. Korotun and V. V. Pogosov, *Phys. Solid State*, **63,** No. 1: 122 (2021).

6.   R. Otero, A. L. Vázquez de Parga, and R. Miranda, *Phys. Rev. B*, **66,** No. 11: 115401 (2002).

7.   J. J. Paggel, C. M. Wei, M. Y. Chou, D.-A. Luh, T. Miller, and T.-C. Chiang, *Phys. Rev. B*, **66,** No. 23: 233403 (2002).

8.   Y. Liu, J. J. Paggel, M. H. Upton, T. Miller, and T.-C. Chiang, *Phys. Rev. B*, **78,** No. 23: 235437 (2008).

9.   A. L. Vázquez de Parga, J. J. Hinarejos, F. Calleja, J. Camarero, R. Otero, and R. Miranda, *Surf. Sci.*, **603,** No. 10: 1389 (2009).

10. P.-W. Chen, Y.-H. Lu, T.-R. Chang, C.-B. Wang, L.-Y. Liang, C.-H. Lin, C.-M. Cheng, K.-D. Tsuei, H.-T. Jeng, and S.-J. Tang, *Phys. Rev. B*, **84,** No. 20: 205401 (2011).

11. R. Y. Liu, A. Huang, C. C. Huang, C.-Y. Lee, C.-H. Lin, C.-M. Cheng, K.-D. Tsuei, H.-T. Jeng, I. Matsuda, and S.-J. Tang, *Phys. Rev. B*, **92,** No. 11: 115415 (2015).

12. M. V. Kuzmin and M. A. Mitzev, *Fiz. Tverd. Tela*, **65,** No. 7: 1082 (2023) (in Russian).

13. N. E. Singh-Miller and N. Marzari, *Phys. Rev. B*, **80,** No. 25: 235407 (2009).

14. E. Ogando, N. Zabala, E. V. Chulkov, and M. J. Puska, *Phys. Rev. B*, **71,** No. 20: 205401 (2005).

15. L. Gao, J. Souto-Casares, J. R. Chelikowsky, and A. A. Demkov, *J. Chem. Phys.*, **147,** No. 20: 214301 (2017).

16. R. Tran, X.-G. Li, J. H. Montoya, D. Winston, K. A. Persson, and S. P. Ong, *Surf. Sci.*, **687,** No. 1: 48 (2019).

17. P. A. Schultz, *Phys. Rev. B*, **103,** No. 19: 195426 (2021).

18. A. V. Babich and V. V. Pogosov, *Phys. Solid State*, **55,** No. 1: 196 (2013).

19. V. V. Pogosov, A. V. Babich, and P. V. Vakula, *Phys. Solid State*, **55,** No. 10: 2120 (2013).

20. A. V. Babich, *Ukrayins'kyy Fizychnyy Zhurnal*, **59,** No. 1: 38 (2014).

21. V. V. Pogosov and V. I. Reva, *Metallofiz. Noveishie Tekhnol.*, **44,** No. 3: 297 (2022).

22. M. Volkov, S. A. Sato, A. Niedermayr, A. Rubio, L. Gallmann, and U. Keller, *Phys. Rev. B*, **107,** No. 18: 184304 (2023).

23. V. V. Batygin and I. N. Toptygin, *Collection of Problems on Electrodynamics and Special Theory of Relativity* (St. Petersburg−Moskva−Krasnodar: Lan': 2010) (in Russian).

24. Z. Wang and C. Guet, *IEEE Transactions on Emerging Topics in Computational Intelligence*, **6,** No. 3: 429 (2021).

25. W. R. Smythe, *Static and Dynamic Electricity* (CRC Press: 1989).

26. A. M. Teale, T. Helgaker, A. Savin, C. Adamo, B. Aradi, A. V. Arbuznikov, P. W. Ayers, E. J. Baerends, V. Barone, P. Calaminici, E. Cancès, E. A. Carter, P. K. Chattaraj, H. Chermette, I. Ciofini, T. D. Crawford, F. De Proft, J. F. Dobson, C. Draxl, T. Frauenheim, E. Fromager, P. Fuentealba, L. Gagliardi, G. Galli, J. Gao, P. Geerlings, N. Gidopoulos, P. M. W. Gill, P. Gori-Giorgi, A. Görling, T. Gould, S. Grimme, O. Gritsenko, H. Jørgen A. Jensen, E. R. Johnson, R. O. Jones, M. Kaupp, A. M. Köster, L. Kronik, A. I. Krylov, S. Kvaal, A. Laestadius, M. Levy, M. Lewin, S. Liu, P.-F. Loos, N. T. Maitra, F. Neese, J. P. Perdew, K. Pernal, P. Pernot, P. Piecuch,

E. Rebolini, L. Reining, P. Romaniello, A. Ruzsinszky, D. R. Salahub, M. Scheffler, P. Schwerdtfeger, V. N. Staroverov, J. Sun, E. Tellgren, D. J. Tozer, S. B. Trickey, C. A. Ullrich, A. Vela, G. Vignale, T. A. Wesolowski, X. Xu, and W. Yang, *Phys. Chem. Chem. Phys.*, **24: 28700 (2022).**

27. A. V. Babich and V. V. Pogosov, *Surf. Sci.*, **603,** No. 16: 2393 (2009).
28. A. Kiejna and V. V. Pogosov, *Phys. Rev. B*, **62,** No. 15: 10445 (2000).
29. R. Garron, *Ann. Phys.*, **13,** No. 10: 595 (1965).
30. S. A. Nepiiko, *Fizicheskie Svoystva Melkikh Metallicheskikh Chastits* [Physical Properties of Small Metal Particles] (Kiev: Naukova Dumka: 1985) (in Russian).